Surface & Coatings Technology 310 (2017) 256–262

Contents lists available at ScienceDirect

Surface & Coatings Technology

journal homepage: www.elsevier.com/locate/surfcoat

Fabrication and characterization of antimicrobial surface-modified stainless steel for bio-application

Kang-Kyun Wang [1], Bong-Jin Kim [1], Il-Heo [1], Seong-Jin Jung, Jeong-Wook Hwang, Yong-Rok Kim *

Department of Chemistry, Yonsei University, Seoul 03722, Republic of Korea

ARTICLE INFO

Article history:
Received 28 July 2016
Revised 20 December 2016
Accepted in revised form 21 December 2016
Available online 23 December 2016

Keywords:
Photofunctional stainless steel
Antimicrobial property
Reactive oxygen species
Photosensitizer
Surface treatment

ABSTRACT

We report a photofunctional stainless steel (PSS) that has antimicrobial property which is provided by reactive oxygen species (ROS) generated from the photosensitizer (PS). For the fabrication of the photofunctional stainless steel, the photosensitizer of hematoporphyrin (HP) was covalently bonded to the surface of 316L stainless steel (316LSS) through an esterification reaction. The PSS plate was investigated by x-ray photoelectron spectroscopy (XPS), reflectance UV–Vis absorption, and fluorescence spectroscopy. ROS generation from the PSS plate was studied by using the decomposition reaction of 1,3-diphenyl-isobenzofuran (DPBF). The results suggest that the immobilized photosensitizer molecules on the surface of the PSS plate still possess their intrinsic optical and functional properties including the ROS generation. The antimicrobial property of the PSS plate was successfully demonstrated with the decomposition of biofilm and the suppression of the biofilm formation on the surface of the PSS plate.

1. Introduction

Centers for Disease Control and Prevention (CDC) reported that Healthcare-Associated Infections (HAIs) occur while receiving medical treatment in a hospital facility [1]. HAIs such as pneumonia, surgical-site infections, urinary tract infection, and gastrointestinal infections were annually arisen up to 38.1% of 1.7 million hospitalized patients in the US [2,3]. Morbidity or mortality rate of HAIs has been increasing constantly [4] and, particularly, the medical device related infections such as central-catheter-associated bloodstream infection, catheter-associated urinary tract infection, and ventilator-associated pneumonia, etc., have been accounted for 25.6% in HAIs [2]. To prevent the infections, medical devices and materials were commonly sterilized by alcohol solutions, autoclaving, ultraviolet (UV) exposure, and gamma irradiation in most hospitals [5].

However, these methods have the limitations to be applied for the implanted medical materials such as surgical pin, implant-tooth in the body. Also, some medical devices including polymers and/or high sensitive medical instruments cannot be sterilized by alcohols and UV light due to the possible damages to the materials and/or malfunction of medical instruments. To prevent contamination of bacteria, many researches have been performed with the surface modification technologies such as drug coated catheter [6], super-hydrophobic catheter for inhibition of bacterial biofilm [7], enzyme-based antimicrobial materials [8], and metal coating stainless steel, etc., [9,10]. However, the drug-coated biomaterials work only for a limited time of period due to the fixed amount of drug and moreover these drugs may cause the occurrence of new drug-resistance bacteria [11]. Super hydrophobic catheter can be fabricated with various substrates by simple methods. Although they show the efficacy for decomposition of biofilm, it does not have suitability for use in the practical field due to the low cell adhesion efficiency [12]. In the case of the enzyme-based medical devices, they have no toxicity, long-term lifetime, and high antibacterial activity. Nevertheless they cannot be widely applied to the medical field due to the enzyme sensitivity that is easily affected by the environmental condition of pH, temperature, and existence of other enzymes [13]. Finally, in the case of the metal coating stainless steel, it can easily be fabricated by the simple method and low cost. Also, they have the high efficacy for decomposition of biofilm [14]. However, it also has a limitation for the application of the clinical surgery since the continuously activated metal coating stainless steel by liquid can influence not only to the bacteria but also other cells when it is implanted in the body. Recently, ROS are being reported to be very effective tool for the elimination of harmful bacteria including the multi-resistant bacteria [15], Gram-positive bacteria [16], and Gram-negative bacteria [17].

In this study, we demonstrate a simple fabrication of the photofunctional stainless steel plate that generates ROS from the surface of the stainless steel plate. 316LSS is one of the major materials that are widely used for medical materials due to good mechanical properties [18], corrosion resistance [19], low cost and biocompatibility [20]. The generation of ROS from the fabricated PSS plate is confirmed

* Corresponding author at: Department of Chemistry, Yonsei University, 50 Yonsei-ro, Seodaemun-Gu, Seoul 03722, Republic of Korea.
E-mail address: yrkim@yonsei.ac.kr (Y.-R. Kim).
[1] These authors contributed equally.

http://dx.doi.org/10.1016/j.surfcoat.2016.12.088
0257-8972/

with the photocatalytic reactions. In order to check the antimicrobial effect, the decomposition of the formed biofilm and the suppression of the biofilm formation on the surface of the PSS plate are evaluated with the low photon energy of green light emitting diode (GLED, 3.5 mW/cm^2).

2. Experimental

2.1. Preparation of the photofunctional stainless steel plate

Overall process of manufacturing the photofunctional stainless plate is shown in Fig. 1. HP and 316LSS were purchased from Aldrich and Han-Yang Stainless co. Ltd. (Republic of Korea), respectively. The HP solution was prepared at a concentration of 2.1×10^{-3} M in ethanol. The 316LSS plate was cut to a circle form (d = 8 mm, thickness = 0.25 mm) and treated with acetone (Merck, HPLC grade) under ultrasonication for 10 min. The 316LSS plate was, then, washed with hexane (Merck, HPLC grade) and distilled water for 3 times. In order to enhance the hydroxyl groups on the surface of the 316LSS plate, they were immersed in the piranha solution (H_2O_2: H_2SO_4 = (1:3 vol.%), Showa chemical co. Ltd.) for 1 h at 100 °C and then dipped in HNO_3 solution (40%, Matsunoen chemicals Ltd.) for 30 min at 70 °C [21]. For stabilization of hydroxyl group on the surface of the 316LSS plate, they were immersed into boiling H_2O_2 for 30 min [21]. For fabrication of the PSS plates, the oxidized 316LSS plates were reacted with EDC/NHS (Sigma.%, 1:5, TCI/Sigma-Aldrich) for 6 h in the HP solution at room temperature [22]. Then the fabricated PSS plates were washed with ethanol under vigorous stirring condition and dried in the oven at 60 °C for 6 h. For the quantization of the HP molecules bonded to the surface of the oxidized 316LSS plate, the solution after the reaction and the washing solution were collected and O.D. of HP in the solution was measured with UV–Vis spectrophotometer (Hitachi, U-2900, Japan) [23]. Amount of HP bonded to the surface was estimated to be 1.1×10^{-8} mol/cm^2.

2.2. Charcterization of the photofunctional stainless steel plate

X-ray photoelectron spectroscopy (XPS, Thermo VG, Escalab 220i-XL, United Kingdom) was performed in order to confirm the covalent bonding nature between the hydroxyl groups of HP and the hydroxyl groups on the surface of the oxidized 316LSS plate. X-ray source of a monochromated Al X-ray (Al Kα line: 1486.6 eV) and 12 kV were utilized, and the compositional survey and detailed scans were acquired using pass energy of 100 eV with 1 eV stepwise and 50 eV with 0.1 eV stepwise [23,24]. The binding energies were corrected by referencing the C 1s binding energy of 285 ezV. In order to evaluate thickness of the covalently bonded HP molecular layer on surface of the stainless steel plate, an atomic force microscope (AFM, Nanowizard-I, JPK instrument, Germany) topography image was obtained in non-contact mode with the HP molecular layer partially bonded to the surface of PSS (scan range: XY: 0–100 μm; Z: 0–15 μm, noise level: XY < 0.02 nm RMS, Z < 0.035 nm RMS). The hardness of PSS was measured with the nano-indentation technique (MTS XP, MTS Systems Co., USA) [25]. The indentation was made to a maximum depth of 100 nm (with a maximum load of about 500 mN) and under a strain rate of 0.05 s^{-1}. Steady state absorption spectra of the HP solution and the PSS plate were obtained with a UV–Vis spectrophotometer (Hitachi, U-2900, Japan) and a diffuse reflectance UV–Vis spectrophotometer (Jasco, V-550, Japan) equipped with an integrating sphere to avoid the scattering of the 316LSS plate, respectively [23]. Steady state emission spectra of the HP solution and the PSS plate were obtained with a spectrofluorimeter (Hitachi, F-4500, Japan).

2.3. Reactive oxygen generation from the photofunctional stainless steel plate

For the confirmation of ROS generation from the PSS plate, degradation of 1,3-diphenylisobenzofuran (DPBF, Sigma-Aldrich) of a reactive oxygen quencher was studied with the PSS plate [23]. The PSS plate was introduced into DPBF solution (2 mL, 1.0×10^{-5} M, ethanol) in the dark condition. The light source for irradiation to the PSS plate was green light emitting diode (GLED, λ_{max} = 520 nm, FWHM = 40 nm, 3.5 mW/cm^2, Itswell Co. Ltd., Republic of Korea). The total output power for the irradiation was measured with a laser power meter (Ophir-opironics Ltd., Nova, Israel). At every 10 min of irradiation, the absorption spectra of DPBF were monitored with a UV–Vis spectrophotometer (Hitachi, U-2900, Japan) [23,24].

2.4. Antimicrobial effect of the photofunctional stainless steel plate

In order to check the photodynamic antimicrobial effect of the PSS plate, the decomposition efficiency of the formed biofilm and the suppression efficiency of the biofilm formation on the surface of the PSS plate were evaluated [24]. The ROS generation was done by irradiation of the GLED (λ_{max} = 520 nm, FWHM = 40 nm, 3.5 mW/cm^2) light onto the PSS plate through a cut-off filter (<400 nm, CVI, USA) which blocked the residual UV light from GLED. Power density of the GLED light was measured at the sample position by a light power meter (Ophir-opironics Ltd., Nova, Israel). For the photodynamic antimicrobial study of the PSS plate, *Staphylococcus aureus* (*S. aureus*, ATCC 25923)

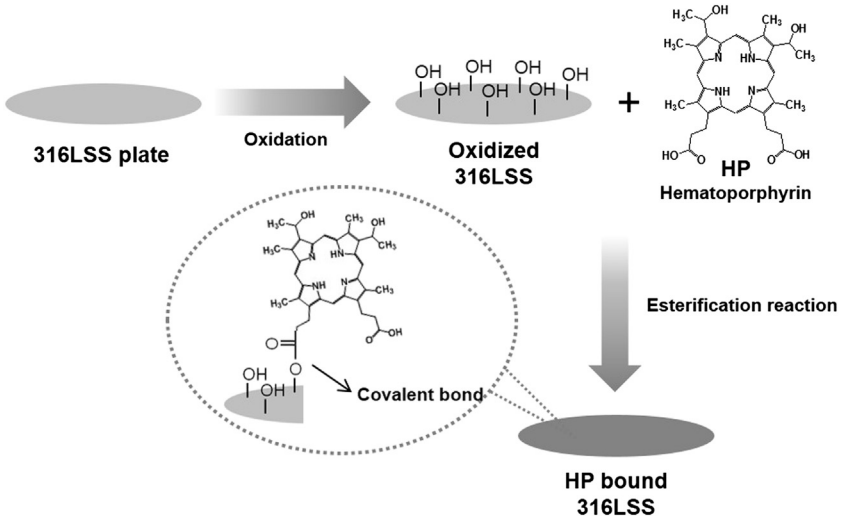

Fig. 1. Fabrication of the PSS plate.

Table 1
Chemical composition.[a]

Elements	Cr	Fe	C	Ni	Si
Atomic %	16.6	Balance	0.018	10.1	0.38

[a] Provided by Han Yang Stainless Co. Ltd., Republic of Korea.

and *Escherichia coli* (*E. coli*, ATCC 25922) were used. The bacteria were aerobically grown in Luria Bertani media (LB) broth (Becton Dickinson; BD, LB broth) at 37 °C for 24 h [24]. These bacteria were diluted in PBS and the resulting bacterial suspensions approximately contained 2.5×10^8 cfu/mL. Number of the bacteria was determined with a turbidity meter (Biomerieux, DensiCHEK plus, USA). For the formation of the biofilm on the surface of the PSS plate, the PSS plate was immersed in the bacterial solution (2 mL) under a dark condition at 37 °C for 24 h [24,26]. Then, the PSS plate was washed with PBS (Life technologies, USA) for 3 times. The biofilm formation on the surface of the PSS plate was verified by the existence of the extracellular polymeric substance (EPS) stained with a Texas Red-conjugated concanavalin A (Life technologies, USA) which was observed by fluorescence microscopy (Carl Zeiss, Axio imager Z2m, Germany) [23,27]. For the decomposition of the biofilm on the surface of the PSS plate, the biofilm formed PSS plates were placed in the 48-well plate with PBS (1 mL) and then the GLED light (3.5 mW/cm^2) was irradiated to the biofilm formed PSS plates for 20, 40, 60, 80, 100, and 120 min. Then, the PSS plates were washed with PBS to remove non-adhesive residual bacteria on the surface of the PSS plate except the biofilm on the PSS plate. The PSS plates were immersed in 1 mL of PBS with a strong agitation for 10 min [24,28]. 100 mL of the suspension was inoculated on the blood agar plates (*S. aureus*)/MacConkey agar (*E. coli*) plates. After aerobically incubation at 37 °C for 24 h, the bacteria colonies were counted. For the suppression study of the biofilm formation on the surface of the PSS plate, the PSS plates were placed in the 48-well plate with bacterial solution (1 mL) and then the GLED light was irradiated to the PSS plates for 12, 24, 36, and 48 h. Then, the PSS plates were examined with the same procedure as above.

3. Results and discussion

The chemical composition of used alloy provide from Han Yang Stainless Co. Ltd. (Republic of Korea) as shown in Table 1. XPS study was performed to confirm that HP is covalently bonded to the surface of the 316LSS plate. Fig. 2 presents the XPS spectra over the binding energy range of 528–718 eV for (a) the 316LSS plate, (b) the oxidized 316LSS plate, (c) and the PSS plate. The spectra show the characteristic peaks corresponding to Fe $2p_{3/2}$, Cr $2p_{3/2}$ and O 1s that exist in the 316LSS plate. The Fe $2p_{3/2}$ peak in the 316LSS plate could be fitted with three peaks at 707.0, 708.0, and 710.5 eV, which were the typical ones of metallic Fe, Fe_3O_4, and Fe_2O_3, respectively [29]. In the Cr $2p_{3/2}$ region, metallic Cr, Cr_2O_3, $Cr(OH)_3$, and CrO_3 are presented at 574.0, 576.1, 577.3, and 578.8 eV, respectively [30]. The peaks of Fe3O4 at 708.0 eV and FeOOH at 712.5 eV for the oxidized 316LSS plate are significantly

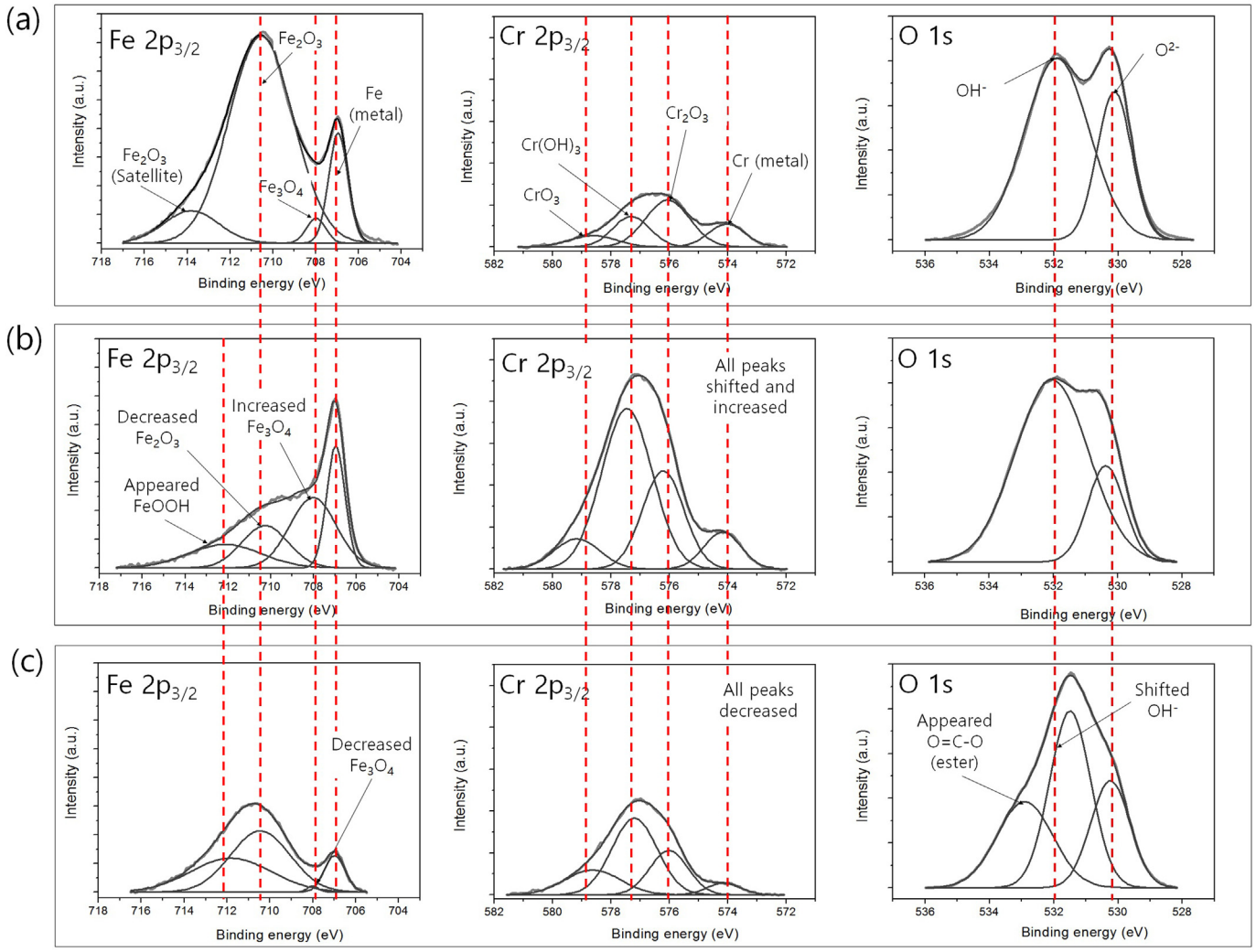

Fig. 2. XPS analyses of (a) the pure 316LSS plate, (b) the oxidized 316LSS plate, and (c) the PSS plate.

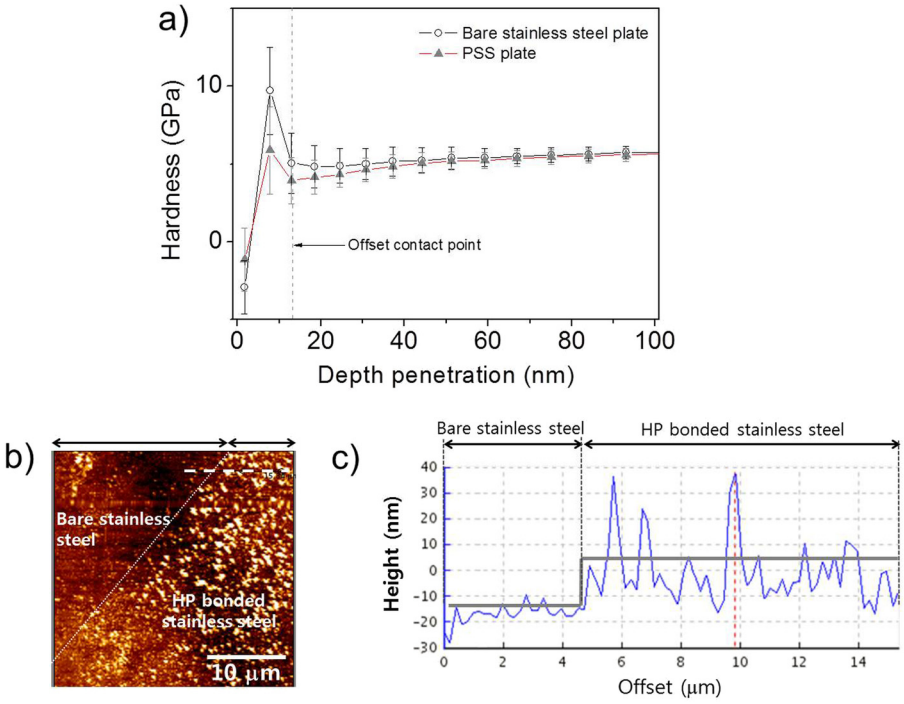

Fig. 3. (a) Hardness vs depth penetration of the bare stainless steel plate (empty circle, black line) and the PSS plate (filled triangle, red line) (b) non-contact mode AFM topography image of the HP molecular layer partially bonded to the surface of stainless steel plate, (c) 2-dimensional AFM image profile of the dashed line in (b). (For interpretation of the references to color in this figure legend, the reader is referred to the web version of this article.)

increased and appeared due to the Fe oxide layer formed on the surface of the 316LSS plate [29,31]. The binding energies of Cr 2p for the oxidized 316LSS plate are slightly shifted to higher energy than those of the 316LSS plate because the Cr oxides are strongly hydroxylated by the chemical treatment [32]. The peaks of Cr 2p at 574.2, 576.3, 577.8, and 579.5 eV for the PSS plate are significantly decreased and the ester peak of O 1s for the PSS plate is appeared at 533.0 eV [33]. In more details, the peak at 533 eV is attributed to the presence of O═C-O resulted from the esterification reaction between the hydroxyl group on surface of the oxidized 316LSS plate and the carboxylic acid group of the HP molecules [34]. The binding energy of O 1s at 531 eV for the PSS plate is slightly shifted to lower energy than the case of the 316LSS plate due to the decreased electron density on the surface of the oxidized 316LSS plate by the electron transfer from HP molecules to the oxidized 316LSS [35]. Such tendency is in a good agreement with the reported values of the oxidized 316LSS plate and other organic compounds bonded to the 316LSS plate [36].

As shown in the Fig. 3a, hardness of the PSS plate increases at the offset contact point of 15 nm until 35 nm of the depth penetration. After 35 nm of the depth penetration, the hardness of PSS (3.9 ± 1.4 GPa) is similar to or slightly less than that of the bare stainless steel plate (5.0 ± 1.9 GPa) within the error range. From the results, the thickness of the covalently bonded HP molecular layer on the surface of stainless steel is approximately expected to be <20 nm, which well correlates to the thickness of 12 nm estimated from the AFM result of Fig. 3c. Moreover, as stated in the references [37,38], the introduced organic molecules to the inorganic components in the surface of metal by the covalent bonding tend to have the good scratched resistance, mechanical strength, and durability.

Diffuse reflectance UV–Vis absorption spectrum of the PSS plate is shown in Fig. 4a together with the absorption spectrum of HP molecules in THF for the comparison. The spectrum of HP solution shows that one B band (400 nm) and four Q bands (498, 530, 569, 623 nm) [39]. The diffuse reflectance absorption spectrum of the PSS plate also includes B and Q bands at the similar wavelengths with the broad shapes and the red shifted peak positions. Such differences in the peak width and position are possibly due to the self-coupling of HP molecules bonded to the surface and the inhomogeneous bonding nature of HP molecules on the surface of the 316LSS plate [40]. The fluorescence spectrum of HP ($\lambda_{ex} = 400$ nm) solution in Fig. 4b presents the peaks at 623 nm and 687 nm, the PSS plate provide the slightly blue-shifted peaks at 618 and 675 nm. The blue-shifted emission peaks are attributed to the strong bonding between the HP molecules and the 316LSS plate [41]. Therefore, the results suggest that HP molecules are covalently bonded

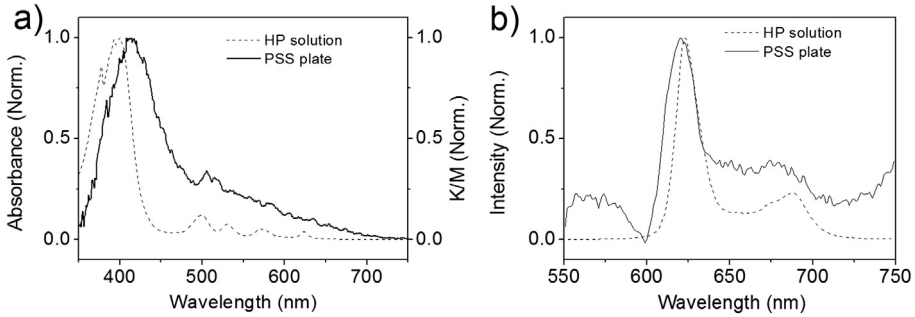

Fig. 4. (a) Absorption and (b) emission spectra of HP in THF solvent (dashed line) and the PSS plate (solid line).

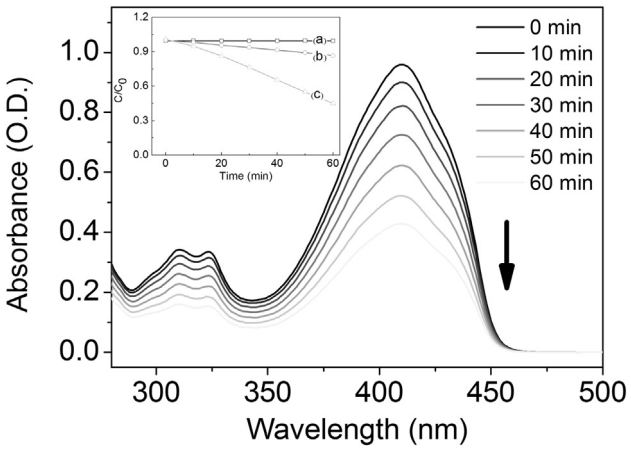

Fig. 5. Reaction time dependent UV–Vis spectra of DPBF in the presence of the PSS plate in EtOH solution with GLED irradiation. Inset represents the ratio between the O.D. (C) after the reaction and the initial O.D. (C_0) of DPBF as function of irrradiation time: (a) DPBF with the PSS plate under dark condition (b) DPBF only with the light, (c) DPBF with the PSS plate with the light. All measurements were performed with the same power of the light irradiation.

to the surface of the oxidized 316LSS plate through the esterification reaction without a change of its photophysical property.

In order to prove the ROS generation from the PSS plate, decomposition study of DPBF of a ROS quencher was performed with the PSS plate. DPBF readily undergoes 1,4-cycloaddition reaction with singlet oxygen to form the endoperoxides and then decomposes into the irreversible products (1,2-dibenzoylbenzene) [42]. Also, it is reported that DPBF can be decomposed by super oxide anion radical of ROS [43]. These decomposition reactions can easily be observed by measuring the decrease in optical density of the DPBF absorption at 415 nm. Fig. 5 indicates the decomposition rate of DPBF as a function of irradiation time in the presence of the PSS plate. The result shows that the light only and the PSS plate with light induce the decomposition of DPBF whereas DPBF does not show any degradation in the presence of the PSS plate without the light irradiation.

To evaluate the photodynamic antimicrobial effect of the PSS plate, a Gram-positive bacterium of *S. aureus* (ATCC 25923) and a Gram-negative bacterium of *E. coli* (ATCC 25922) were used. Formation of the *S. aureus* and the *E. coli* biofilm on the surface of the PSS plate were observed by fluorescence microscope. EPS was visualized by staining with a Texas Red-conjugated concanavalin A as shown in Fig. 6. Number of *S. aureus* was effectively decreased from 10^5 CFU/mL to 10^0 CFU/mL (Fig.7a), whereas that of *E. coli* was decreased only from 10^6 CFU/mL to 10^4 CFU/mL (Fig.7b) within 2 h with GLED irradiation condition of 3.5 mW/cm^2. The result suggests that a Gram-negative bacterium of *E. coli* was less influenced by ROS than a Gram-positive bacterium of *S. aureus*. It is explained that the lipopolysaccharide (LPS) on the surface of *E. coli* are the efficient quenching site to ROS generated from the PSS plate [44]. Both cases of biofilm were decomposed by the PSS plate with the low dose of light although the efficiency of bactericidal effect somewhat depended on the type of bacteria.

In order to check the suppression effect of the biofilm formation on the surface of the PSS plate, the PSS plate within *S. aureus* or *E. coli* solution was continuously irradiated by 3.5 mW/cm^2 of GLED light since the PSS plate was initially put into of the bacterial solution. After 12, 24, 36, and 48 h, the surfaces of the PSS plates were analysed in order to check the formation of biofilms. As shown in Fig. 8a, *S. aureus* solution did not result any of the biofilm formation on the surface of the PSS plate. In the case of *E. coli* solution, number of bacteria was ranged from 10^0 CFU/mL to 10^2 CFU/mL within the total incubation time of 48 h. It also suggests that *E. coli* is less influenced by ROS than *S. aureus* due to the same reason as the case of the biofilm PDI results above [45]. Therefore, it is expected that the case of *E. coli* requires more irradiation power for the prevention and the suppression.

4. Conclusions

The photofunctional stainless steel (PSS) plate with antimicrobial property is successfully fabricated by a simple surface modification process of the 316LSS plate and the esterification reaction with HP. The XPS, UV–Vis, and emission spectra indicate that the HP molecules are covalently bonded to the surface of the 316LSS plate. Photo-induced ROS generation from the PSS plate is demonstrated with the DPBF decomposition study. Moreover the antimicrobial effect of the PSS plate was tested with *S. aureus* and *E. coli*. Under the given condition of experiment, especially, the formed biofilm by *S. aureus* was effectively decomposed (99.999%) by the ROS generated from the PSS. And the biofilm formation by *S. aureus* was completely inhibited for 2 day under the condition of light irradiation. Therefore, the photofunctional stainless steel with effective antimicrobial effect can be applied to various practical applications utilizing stainless steel such as antimicrobial instrument, antimicrobial cooking utensil, and sterilization goods.

Conflict of interest

The authors declare that there is no conflict of interests regarding to the publication of this paper.

Acknowledgments

This work was carried out with the support of "Cooperative Research Program for Agriculture Science & Technology Development (Project No. PJ01083001)" Rural Development Administration, Republic of Korea and the National Research Foundation of Korea (NRF) funded by the Ministry of Science, ICT & Future Planning (grant No. 2012M3A9C6049729).

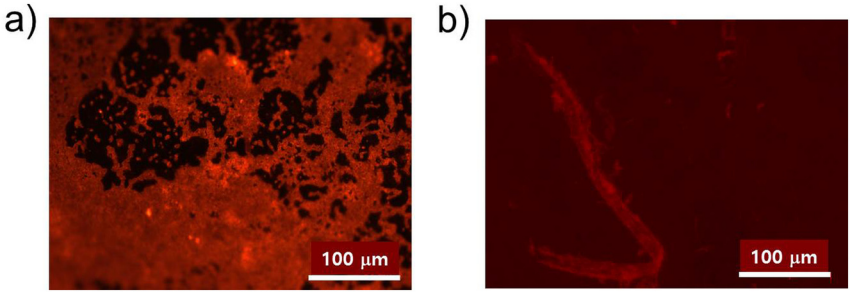

Fig. 6. Fluorescence microscope images of (a) *S. aureus* biofilm, and (b) *E. coli* biofilm on the surface of the PSS plate after pre-incubation for 24 h: EPS was stained with Texas Red-conjugated concanavalin A (λ_{ex} = 545 nm). (For interpretation of the references to color in this figure legend, the reader is referred to the web version of this article.)

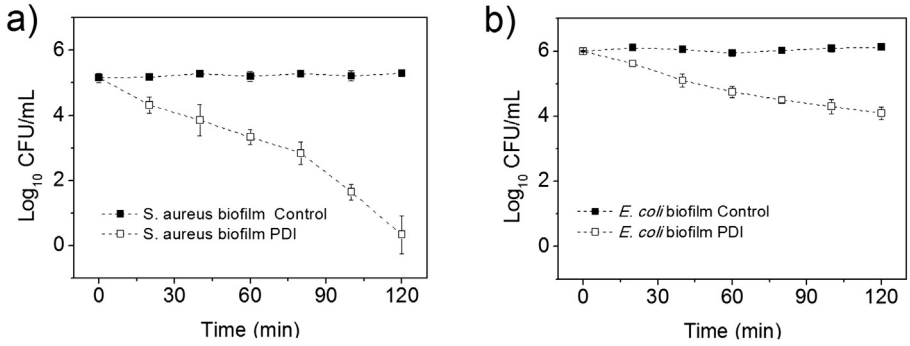

Fig. 7. Survival rates of (a) *S. aureus* (empty square symbol, dot line), and (b) *E. coli* (empty square symbol, dot line) on the surface of the PSS plate after pre-incubation for 24 h: Control (w/o light), PDI (w/ light, GLED 3.5 mW/cm^2). The experiments were repeated by 3 times.

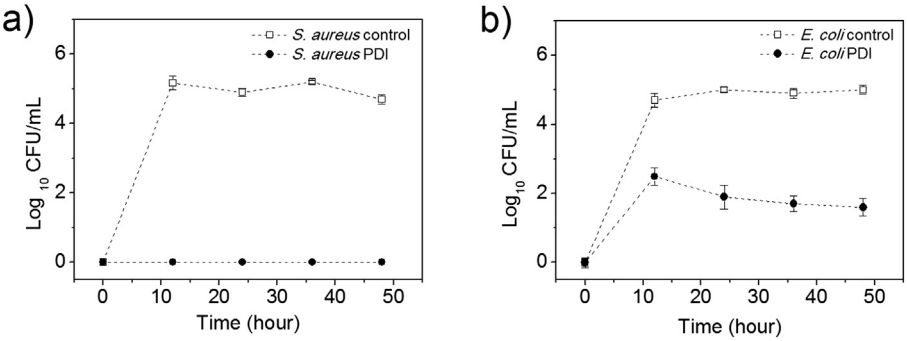

Fig. 8. Viabilities of (a) *S. aureus*, and (b) *E. coli* on the surface of the PSS plate without pre-incubation: Control (w/o light, 24 h incubation, blank square symbol), PDI (w/ light, 3.5 mW/cm^2 of GLED light, 48 h incubation, filled circle symbol). The experiments were repeated by 3 times.

References

[1] Centers for Disease Control and Prevention, National and State Healthcare-Associated Infections Progress Report, 2014 (Published March 2016. Available at www.cdc.gov/hai/progress-report/index.html).

[2] S.S. Magill, J.R. Edwards, M. Stat, W. Bamberg, Z.G. Beldavs, G. Dumyati, M.A. Kainer, R. Lynfield, M. Maloney, L. McAllister-Hollod, J. Nadle, S.M. Ray, D.L. Thompson, L.E. Wilson, S.K. Fridkin, Multistate point-prevalence survey of Healthcare-Associated Infections, N. Engl. J. Med. 370 (2014) 1198–1208.

[3] M.P. Muller, C. MacDougall, M. Lim, I. Armstrong, A. Bialachowski, S. Callery, W. Ciccotelli, M. Cividino, J. Dennis, S. Hota, G. Garber, J. Johnstone, K. Katz, A. McGeer, V. Nankoosingh, C. Richard, M. Vearncombe, Antimicrobial surfaces to prevent healthcare associated infections: a systematic review, J. Hosp. Infect. 92 (2015) 1–7.

[4] S. Hugonnet, H. Sax, P. Eggimann, J.C. Chevrolet, D. Pittet, Nosocomial bloodstream infection and clinical sepsis, Emerg. Infect. Dis. 10 (2004) 76–81.

[5] J. Irudayaraj, Biomedical Nanosensors, Pan Stanford Publishing, 2012.

[6] M.C. Berg, H. Kolodziej, B. Cremers, G. Gershony, U. Speck, Drug-coated angioplasty balloon catheters: coating compositions and methods, Adv. Eng. Mater. 14 (2012) B45–B50.

[7] D. Campoccia, L. Montanaro, C.R. Arciola, A review of the biomaterials technologies for infection-resistant surfaces, Biomaterials 34 (2013) 8533–8554.

[8] T. Yuliana, K. Ebihara, M. Suzuki, C. Shimonaka, S. Amachi, A novel enzyme-based antimicrobial system comprising iodide and a multicopper oxidase isolated from Alphaproteobacterium strain Q-1, Appl. Microbiol. Biotechnol. 99 (2015) 10011–10018.

[9] L. Ren, K. Yang, L. Guo, H. Chai, Preliminary study of anti-infective function of a copper bearing stainless steel, Mater. Sci. Eng. C 32 (2012) 1204–1209.

[10] R. Chen, H. Ni, H. Zhang, G. Yue, W. Zhan, P. Xiong, A preliminary study on antibacterial mechanisms of silver ions implanted stainless steel, Vacuum 89 (2013) 249–253.

[11] B.J. Privett, J. Youn, S.A. Hong, J. Lee, J. Han, J.H. Shin, M.H. Schoenfisch, Antibacterial fluorinated silica colloid superhydrophobic surfaces, Langmuir 27 (2011) 9597–9601.

[12] L. Wang, Y. Han, K. Yang, M. Chen, H. Lin, C. Lin, Y. Hsu, Hydrophilic/hydrophobic surface of Al_2O_3 thin films grown by thermal and plasma-enhanced atomic layer deposition on plasticized polyvinyl chloride (PVC), Surf. Coat. Technol. 305 (2016) 158–164.

[13] L. Betancor, H.R. Luckarift, Bioinspired enzyme encapsulation for biocatalysis, Trends Biotechnol. 26 (2008) 566–572.

[14] M. Hans, J.C. Támara, S. Mathews, B. Baxa, A. Hegetschweiler, R. Kautenburger, M. Solioz, F. Mücklich, Laser cladding of stainless steel with a copper–silver alloy to generate surfaces of high antimicrobial activity, Appl. Surf. Sci. 320 (2014) 195–199.

[15] X. Wang, D. Jia, Y. Liang, S. Yan, Y. Ding, L. Chen, Z. Shi, M. Zeng, G. Liu, L. Fu, Lgf-YL-9 induces apoptosis in human epidermoid carcinoma KB cells and multidrug resistant KBv200 cells via reactive oxygen species-independent mitochondrial pathway, Cancer Lett. 249 (2007) 256–270.

[16] N. Jiang, N.S. Tan, B. Ho, J.L. Ding, Respiratory protein-generated reactive oxygen species as an antimicrobial strategy, Nat. Immunol. 8 (2007) 1114–1122.

[17] W. He, H. Kim, W.G. Wamer, D. Melka, J.H. Callahan, J. Yin, Photogenerated charge carriers and reactive oxygen species in ZnO/Au hybrid nanostructures with enhanced photocatalytic and antibacterial activity, J. Am. Chem. Soc. 136 (2014) 750–757.

[18] M. Jokar, S. Darvishi, R. Torkaman, M. Kharaziha, M. Karbasi, Corrosion and bioactivity evaluation of nanocomposite PCL-forsterite coating applied on 316L stainless steel, Surf. Coat. Technol. 307 (2016) 324–331.

[19] A.A. Ahmed, M. Mhaede, M. Basha, M. Wollmann, L. Wagner, The effect of shot peening parameters and hydroxyapatite coating on surface properties and corrosion behavior of medical grade AISI 316L stainless steel, Surf. Coat. Technol. 280 (2015) 347–358.

[20] C. Ruan, T. Bayer, S. Meth, C.N. Sukenik, Creation and characterization of *n*-alkylthiol and *n*-alkylamine self-assembled monolayers on 316L stainless steel, Thin Solid Films 419 (2002) 95–104.

[21] M.N. Ismail, T.L. Goodrich, Z. Ji, K.S. Ziemer, J. Warzywoda, A. Sacco Jr., Assembly of titanosilicate ETS-10 crystals on organosilane-functionalized gallium nitride surfaces, Microporous Mesoporous Mater. 118 (2009) 245–250.

[22] C. Wang, Q. Yan, H. Liu, X. Zhou, S.-J. Xiao, Different EDC/NHS activation mechanisms between PAA and PMAA brushes and the following amidation reactions, Langmuir 27 (2011) 12058–12068.

[23] K.K. Wang, B.J. Kim, M.H. Lee, B.J. Kwon, D.H. Choi, J.C. Park, Y.R. Kim, Photofunctional Co-Cr alloy generating reactive oxygen species for photodynamic applications, Int. J. Photoenergy 2013 (2013), 618062. (8 pages).

[24] K.K. Wang, S.J. Jung, J.W. Hwang, B.J. Kim, D.H. Kim, I.K. Bae, S.H. Jeong, Y.R. Kim, Bactericidal effect through non-uptake pathway with photofunctional silicon polymer that generates reactive oxygen species, J. Photochem. Photobiol., A 316 (2016) 52–58.

[25] J. Ballarre, E. Jimenez-Pique, M. Anglada, S.A. Pellice, A.L. Cavalieri, Mechanical characterization of nano-reinforced silica based sol–gel hybrid coatings on AISI 316L stainless steel using nanoindentation, Surf. Coat. Technol. 203 (2009) 3325–3331.

[26] M. Shakibaie, H. Forootanfar, Y. Golkari, T. Mohammadi-Khorsand, M.R. Shakibaie, Anti-biofilm activity of biogenic selenium nanoparticles and selenium dioxide against clinical isolates of *Staphylococcus aureus*, *Pseudomonas aeruginosa*, and *Proteus mirabilis*, J. Trace Elem. Med. Biol. 29 (2015) 235–241.

[27] F. Cieplik, A. Späth, J. Regensburger, A. Gollmer, L. Tabenski, K. Hiller, W. Bäumler, T. Maisch, G. Schmalz, Photodynamic biofilm inactivation by SAPYR—an exclusive singlet oxygen photosensitizer, Free Radic. Biol. Med. 65 (2013) 477–487.

[28] X. Qi, P. Gunawan, R. Xu, M.W. Chang, Cefalexin-immobilized multi-walled carbon nanotubes show strong antimicrobial and anti-adhesion properties, Chem. Eng. Sci. 84 (2012) 552–556.

[29] M. Santamaria, F.D. Franco, F.D. Quarto, M. Pisarek, S. Zanna, P. Marcus, Photoelectrochemical and XPS characterization of oxide layers on 316L stainless steel grown in high-temperature water, J. Solid State Electrochem. 19 (2015) 3511–3519.
[30] T. Hanawa, S. Hiromoto, A. Yamamoto, D. Kuroda, K. Asami, XPS characterization of the surface oxide film of 316L stainless steel samples that were located in quasi-biological environments, Mater. Trans. 43 (2002) 3088–3092.
[31] A. Latifi, M. Imani, M.T. Khorasani, M.D. Joupari, Plasma surface oxidation of 316L stainless steel for improving adhesion strength of silicon rubber coating to metal substrate, Appl. Surf. Sci. 320 (2014) 471–481.
[32] M. Minier, M. Salmain, N. Yacoubi, L. Barbes, C. Methivier, S. Zanna, C. Pradier, Covalent immobilization of lysozyme on stainless steel Interface spectroscopic characterization and measurement of enzymatic activity, Langmuir 21 (2005) 5957–5965.
[33] X. Yanlong, Z. Lei, S. Yongfeng, L. Ning, L. Yongli, L. Bin, X. Qinghua, H. Chaoliang, C. Xuesi, Surface modification of 316L stainless steel by grafting methoxy poly(ethylene glycol) to improve the biocompatibility, Chem. Res. Chin. Univ. 31 (2015) 651–657.
[34] H.H. Huang, X. Jiang, Z. Zou, W.S. Chin, G.Q. Xu, W.L. Dai, K.N. Fan, J.F. Deng, Potassium adsorption and reaction with water on MgO(100), Surf. Sci. 412 (413) (1998) 555–561.
[35] Z. Jiang, W. Huang, Z. Zhang, H. Zhao, D. Tan, X. Bao, Molybdenum deposition on the thin alumina film: a combinatorial investigation by HREELS, XPS and UPS, Chem. Phys. Lett. 439 (2007) 313–317.
[36] Y. Xiao, L. Zhao, Y. Shi, N. Liu, Y. Liu, B. Liu, Q. Xu, C. He, X. Chen, Surface modification of 316L stainless steel by grafting methoxy poly(ethylene glycol) to improve the biocompatibility, Chem. Res. Chin. Univ. 31 (2015) 651657.
[37] Y.S. Choi, J.S. Lee, J.G. Han, Scratch-resistant hydrophobic and oleophobic coatings prepared by simple PECVD method, J. Mater. Sci. 49 (2014) 4790–4795.
[38] M. Hu, D. Zhang, Preparation and properties of triazine dithiol-silane composite self-assembled hydrophobility films on stainless steel surfaces, Mater. Sci. Forum 809–810 (2015) 554–562.
[39] K.K. Wang, M.S. Jung, K.H. Choi, H.W. Shin, S.I. Oh, J.E. Im, D.H. Kim, Y.R. Kim, Fabrication and photophysical properties of singlet oxygen generating nanoporous membrane, Surf. Coat. Technol. 205 (2011) 3905–3908.
[40] B.A. Gregg, M.A. Fox, A.J. Bard, Effects of order on the photophysical properties of the liquid crystal zinc octakis(beta-octoxyethyl)porphyrin, J. Phys. Chem. 93 (1989) 4221–4234.
[41] X. Yang, R. Lu, H. Zhou, P. Xue, F. Wang, P. Chen, Y. Zhao, Aggregation-induced blue shift of fluorescence emission due to suppression of TICT in a phenothiazine-based organogel, J. Colloid Interface Sci. 339 (2009) 527–532.
[42] S.R. Harper, M.C. Pfrunder, L.J. Esdaile, P. Jensen, J.C. McMurtrie, D.P. Arnold, Synthetic, structural, and spectroscopic studies of bis(porphyrinzinc) complexes linked by two-atom conjugating bridges, Eur. J. Org. Chem. 2015 (2015) 2807–2825.
[43] Y. Yuan, G. Feng, W. Qin, B.Z. Tang, B. Liu, Targeted and image-guided photodynamic cancer therapy based on organic nanoparticles with aggregation-induced emission characteristics, Chem. Commun. 50 (2014) 8757–8760.
[44] G.K. Harris, Y. Qian, S.S. Leonard, D.C. Sbarra, X. Shi, Luteolina and chrysin differentially inhibit cyclooxygenase-2 expression and scavenge reactive oxygen species but similarly inhibit prostaglandin-E2 formation in RAW 264.7 cells, J. Nutr. 136 (2006) 1517–1521.
[45] T. Maisch, T. Shimizu, Y. Li, J. Heinlin, S. Karrer, G. Morfill, J.L. Zimmermann, Decolonisation of MRSA, *S. aureus* and *E. coli* by cold-atmospheric plasma using a porcine skin model in vitro, PLoS One 7 (2012), e34610. .